

1 Remapping **annual** precipitation in mountainous area based 2 on vegetation pattern: **a case study in the Nu River basin**

3 Xing Zhou¹, Guang-Heng Ni¹, Chen Shen¹, Ting Sun¹

4
5 1) State Key Laboratory of Hydro-Science and Engineering, Department of Hydraulic Engineering, Tsinghua
6 University, Beijing 100084, China

7 *Corresponding to:* Ting Sun (sunting@tsinghua.edu.cn)

8
9 **Abstract.** Accurate high-resolution estimates of precipitation are vital to improve the understanding on basin-
10 scale hydrology in mountainous areas. The traditional interpolation methods or satellite-based remote sensing
11 products are known to have limitations in capturing spatial variability of precipitation in mountainous areas. In
12 this study, we develop a fusion framework to improve the **annual** precipitation estimation in mountainous areas
13 by jointly utilizing the satellite-based precipitation, gauge measured precipitation and vegetation index. The
14 development consists of vegetation data merging, vegetation response establishment, and precipitation remapping.
15 The framework is then applied to the mountainous area of Nu River basin for precipitation estimation. The results
16 demonstrate the reliability of the framework in reproducing the high-resolution precipitation regime and capturing
17 its high spatial variability in the Nu River basin. In addition, the framework can significantly reduce the errors in
18 precipitation estimates as compared with the inverse distance weighted (IDW) method and TRMM (Tropical
19 Rainfall Measuring Mission) precipitation product.

20 21 **1 Introduction**

22 Precipitation plays an important role in hydrological process, land-atmospheric processes, and ecological
23 dynamics. Accurate high-resolution precipitation is crucial for streamflow prediction, flood control, and water
24 resources management in data-sparse regions such as mountainous areas (Song et al., 2015). However, it is of
25 great challenge to obtain accurate precipitation in mountainous areas due to the sparse gauge network and the
26 remarkable spatiotemporal variability of precipitation. Conventional gauge networks can provide accurate rainfall
27 measurements at point scales, which can be interpolated within the region of interest to give estimates of

28 precipitation in ungauged areas. However, such interpolated estimates might not be reliable in mountainous areas
29 considering the very limited gauges there (Phillips et al., 1992; Mair and Fares, 2011; Jacquin and Soto-Sandoval,
30 2013; Wang et al., 2014; Borges et al., 2016).

31
32 Recently, remote-sensing-based precipitation (RSBP) products, such as the Global Precipitation Climatology
33 Project (GPCP) (Schamm et al., 2014), the Tropical Rainfall Measuring Mission (TRMM) (Council, 2005), and
34 the Climate Prediction Center Morphing Method (CMORPH) (Joyce et al., 2004), have been extensively used in
35 ungauged or sparsely-gauged areas to bridge the gap between the need for precipitation estimate and the scarcity
36 in gauge observations (Akbari et al., 2012; Kneis et al., 2014; Li et al., 2015; Worqlul et al., 2015; Mourre et al.,
37 2016; Wong et al., 2016). Also, data fusion across satellite and gauge observations is being conducted to further
38 the application of RSBPs (Rozante et al., 2010; Woldemeskel et al., 2013; Arias-Hidalgo et al., 2013; Chen et al.,
39 2016; Zhou et al., 2016). However, due to the relatively coarse spatial resolution (e.g., 0.25 °-5 °) and uncertainties
40 of RSBPs, their applications in mountainous basins, where the precipitation shows large spatial variability, are
41 still very limited (Krakauer et al., 2013; Chen and Li, 2016).

42
43 Precipitation estimates can be influenced by a variety of ambient factors (e.g., topography, vegetation, etc.). In
44 order to correct effects of topography in precipitation estimate, Digital Elevation Model (DEM) has been widely
45 used in spatial interpolation of precipitation over mountainous areas (Marquínez et al., 2003; Lloyd, 2005).
46 However, the relationship between elevation and precipitation is not clear. Meanwhile, strong correlations
47 between NDVI and precipitation are found by several studies (Li et al., 2002; Kariyeva and Van Leeuwen, 2011;
48 Li and Guo, 2012; Sun et al., 2013; Campo-Bescós et al., 2013). As such, establishing statistical models between
49 normalized difference vegetation index (NDVI) and precipitation so as to improve the spatial resolution of TRMM
50 products in mountainous areas is becoming popular (Immerzeel et al., 2009; Jia et al., 2011; Duan and
51 Bastiaanssen, 2013; Chen et al., 2014; Xu et al., 2015; Mahmud et al., 2015; Jing et al., 2016). For instance,
52 Immerzeel et al. (2009) downscaled TRMM-3B43 to 1 km based on an exponential relationship between NDVI
53 and TRMM precipitation in Iberian Peninsula of Europe. Jia et al. (2011) established four multivariable linear
54 regression models between TRMM-3B43 precipitation and two other factors (i.e., DEM and NDVI) of different
55 resolutions (0.25 °; 0.5 °; 0.75 °; 0.1 °) to get 1 km estimates of precipitation in the Qaidam Basin of China. Duan and
56 Bastiaanssen (2013) used nonlinear relationship between TRMM-3B43 and NDVI to downscale precipitation to

57 1 km in a humid area and a semi-arid area. Chen et al. (2014) established spatially varying relationship among
58 TRMM, NDVI, and DEM by using a local regression analysis approach known as geographically weighted
59 regression (GWR) in South Korea. Xu et al. (2015) also used the GWR method to explore the spatial heterogeneity
60 of the RSBP-NDVI and RSBP-DEM relationships over two mountainous area in western China.

61

62 However, the present RSBP-NDVI-based schemes have several limitations: 1) significant errors can be introduced
63 during the downscaling given the nonlinear relationship between RSBP and NDVI; 2) large uncertainties exist in
64 the RSBP for mountainous areas, and 3) inter-comparison of existing NDVI datasets are missing in deriving the
65 RSBP-NDVI relationships. In this study, we develop a fusion framework to obtain more accurate high-resolution
66 estimates of precipitation in mountainous areas based on the relationship between precipitation and vegetation
67 response. More specifically, in addition to RSBP, gauge measurements and different vegetation datasets will be
68 used in this study to overcome the aforementioned limitations in current RSBP-NDVI-based schemes. The paper
69 is organized as follows: section 2 describes the development of the fusion framework; section 3 documents the
70 study area and related datasets; section 4 presents the results of the fusion framework and discusses impacts of
71 different determinants on the performance of fusion framework; and section 5 summarizes this work.

72

73 **2 Framework development**

74 The satellite-gauge-vegetation fusion framework (Fig. 1) involves three stages of development: 1) vegetation data
75 merging, 2) precipitation-vegetation regression, and 3) RSBP product remapping, whose details are described in
76 the following subsections.

77

78 **2.1 vegetation data merging**

79 Vegetation closely interacts with soil moisture and is recognized as a good proxy of precipitation. The remote
80 sensing technique provides us with various high-resolution vegetation products such as NDVI, EVI (enhanced
81 vegetation index), LAI (leaf area index), etc. Among the vegetation indices, NDVI, an indicator of plant density
82 and growth, is chosen as the proxy of precipitation in this study due to its wide availability. Considering the crucial
83 role of NDVI in deriving precipitation estimates under our framework, we conduct an inter-comparison in data

84 accuracy between two NDVI datasets (termed as datasets A and B hereinafter) to reduce the error. First, the
85 systematic errors of both datasets are eliminated by multiplying reduction factor or using simple regression model.
86 After the correction, the final dataset is then obtained by selecting better element between A and B if the quality
87 criteria is satisfied otherwise filling an anomaly value.

88

89 It should be noted that since the vegetation growth is suppressed or promoted on some land covers (e.g. rivers,
90 lakes, snow and ice, and urban areas), the vegetation data of these land covers are excluded by filling anomaly
91 values. Besides, due to the strong influence of farming activities (e.g. irrigation, fertilization, and harvest) on the
92 crop growth, vegetation data of farmland are excluded as well. We note that although Moran's Index (Li et al.,
93 2007) is widely employed to detect anomalies in vegetation data (Jia et al., 2011; Duan et al., 2013), it is not used
94 in this study for its inapplicability in large areas with continuous anomaly pixels (e.g. farmland). As such, we
95 identify anomaly pixels simply by landuse type: pixels categorized as water, wetland, urban, cropland, snow/ice,
96 and barren will be identified as anomalies. The detected anomaly pixels are excluded from the original NDVI
97 dataset and then filled with interpolated values using IDW method so as to generate an optimized NDVI dataset.

98

99 Based on the optimized NDVI dataset, the NDVI data at the gauge locations are retrieved with neighbor-average
100 method (i.e. the value of a certain grid is determined as the average of all its eight neighboring grids) and will be
101 used for the precipitation-vegetation regression.

102

103 **2.2 precipitation-vegetation regression**

104 As far as we know, there is no widely accepted form for the precipitation-vegetation relationship. Therefore, the
105 final regression form will be determined from several candidate relationships, including polynomial, exponential,
106 logarithmic and linear forms, according to the five metrics: correlation coefficient (R), coefficient of determination
107 (R^2), root-mean-square error (E_{RMS}), mean relative error (E_{MR}) and mean absolute relative error (E_{MAR}), which are
108 given as follows:

$$R = \frac{\sum_{i=1}^n (P_i - \bar{P})(O_i - \bar{O})}{\sqrt{\sum_{i=1}^n (P_i - \bar{P})^2} \sqrt{\sum_{i=1}^n (O_i - \bar{O})^2}} \quad (1)$$

$$R^2 = \frac{\sum_{i=1}^n (P_i - O_i)^2}{\sqrt{\sum_{i=1}^n (O_i - \bar{O})^2}} \quad (2)$$

$$E_{\text{RMS}} = \sqrt{\frac{\sum_{i=1}^n (P_i - O_i)^2}{n}} \quad (3)$$

$$E_{\text{MR}} = \frac{1}{n} \sum_{i=1}^n (P_i - O_i) \quad (4)$$

$$E_{\text{MAR}} = \frac{1}{n} \sum_{i=1}^n \frac{|P_i - O_i|}{O_i} \quad (5)$$

109 where \bar{O} is the mean annual precipitation of all gauges, O_i the mean annual precipitation of gauge i , P_i the
 110 estimated precipitation at gauge i , and n the total number of gauges.

111

112 Also, considering the annual variability of precipitation, the regression model is further determined for two
 113 temporal scales: 1) entire period covering all the study years and 2) individual year of the entire study period. The
 114 **Regression Models for Entire study period** and for **Individual years** are thus termed as **RME** and **RMI**,
 115 respectively. RME can utilize the full knowledge of precipitation characteristics of the entire study period, whereas
 116 RMI implies the inter-annual variability. Besides, RME can reasonably reconstruct the precipitation series of the
 117 years when data gaps exist.

118

119 The calibration-validation procedure for each candidate model is conducted under three scenarios with different
 120 numbers of gauge and/or years:

- 121 a) Fully random: random number of gauges and random number of years are independently used for
 122 calibration and validation;
- 123 b) All gauges, partial period: all the gauges will be involved in both procedures, but only 2/3 of years will
 124 be randomly chosen for calibration and the other years for validation;
- 125 c) Partial gauges, entire period: all years will be used, but only 1/3 of gauges will be randomly chosen for
 126 calibration and other gauges for validation.

127 For each scenario, the calibration-validation procedure will be performed for one hundred samples determined
 128 based on the above criteria and the six evaluation metrics (i.e. R , R^2 , E_{RMS} , E_{MA} and E_{MAR}) will be calculated for
 129 each sample accordingly. The best model is then determined based the metrics.

130

131 **2.3 RSBP product remapping**

132 With the optimized vegetation dataset and precipitation-vegetation regression model, the RSBP product is then
133 remapped over the study region. Thanks to the finer resolution of NDVI dataset than RSBP product and the
134 accurate estimate of precipitation by gauges, the remapped RSBP product is expected to provide more detailed
135 spatial characteristics of precipitation over mountainous areas.

136 **3 Study area and datasets for framework application**

137 **3.1 Study area**

138 The Nu-Salween basin (Fig. 2a), where 6 million people are living, is one of the largest river basins in South Asia
139 and spreads across three countries with an area of 324,000 km². This study focuses on the Chinese part of the Nu-
140 Salween basin (termed as the Nu river basin hereafter), where the elevation ranges from 446 m to 6134 m and the
141 narrowest part is only 24 km. The annual precipitation of the Nu river basin ranges from 400 mm to 2000 mm
142 with an average of 900 mm and the mean annual runoff is 69 km³. The precipitation of the Nu river basin generally
143 decreases from southwest to northeast and demonstrates high variability due to mountain weather systems (e.g.
144 the difference in annual precipitation between the mountaintop and valley of Gongshan is larger than 1000 mm).
145 Annual rainfall varies significantly across this region. Fig. 2b shows the annual rainfall distributions of 7 stations
146 located in upstream, middle and downstream of the Nu River basin. The upstream and downstream have similar
147 rainfall distributions with larger rainfall occurs in summer compared to winter while the middle part observes
148 relatively large rainfall in winter and spring. Thanks to the adequate rainfall and minimal human perturbation, the
149 Nu river basin has an extensive vegetation coverage with the dominant type as grassland in the Qinghai-Tibetan
150 Plateau (upper basin) and mixed forest in Yunnan province (lower basin). However, the dense vegetation cover
151 increases the difficulty in conducting precipitation observations and only 13 gauges are very unevenly distributed
152 over the whole basin of 142,479 km², which makes it highly challenging to obtain the accurate spatial precipitation
153 characteristics with traditional interpolation approaches. Although the RSBP products are available for this area,
154 they are too coarse (usually with a spatial resolution of ~50 km) to capture the high spatial variability of
155 precipitation.

156

157 Considering the limited number of gauges (i.e. 13) in the Nu river basin, an enlarged area covering 23°N–33°N
 158 and 91°E–101°E is chosen for the application of the fusion framework, where 59 gauges are available and the
 159 climatic and topographic conditions are similar: both regions are characterized as mountainous areas under the
 160 subtropical climate influenced by southeast and southwest monsoons. Besides, given no rain gauges are available
 161 outside of China in this study region, the non-Chinese region is excluded from the study area.

162

163 3.2 Datasets

164 3.2.1 Vegetation data

165 In this study, we use two MODIS (moderate resolution imaging spectroradiometer) vegetation products,
 166 MOD13A3 (termed MOD hereafter) and MYD13A3 (termed MYD hereafter), in the application of the fusion
 167 framework. Both the MOD and MYD datasets contain 10 sub-datasets consisting of NDVI, EVI and pixel
 168 reliability. The temporal and spatial resolutions of the MOD13A3 and MYD13A3 products are 1 month and 1 km,
 169 respectively. The pixel reliability is an accuracy metric of the data quality pixel and has four valid values: 0 for
 170 good accuracy, 1 for marginal accuracy, 2 for snow/ice, and 3 for cloud. Based on the pixel reliability information,
 171 the NDVI values are either selected for corresponding pixel reliability levels being 0 and 1 or discarded as
 172 anomalies otherwise.

173

174 The MOD dataset is used as benchmark while MYD is taken as the alternative for occasions when MOD data are
 175 missing or have large uncertainties. Since both the MOD and MYD datasets are extracted from different satellites
 176 at different transit times, systematic errors may exist in the difference between the two datasets. As such, we
 177 construct two regressions to remove their systematic errors: one is based on a subset with both MOD and MYD
 178 of good reliability (= 0), and the other on a subset with MOD of marginal reliability (= 1) and MOD of good
 179 reliability (= 0). After the removal of systematic errors, a merged dataset of MOD and MYD (termed MMD
 180 hereafter) is generated under the criteria given as follows:

$$MMD = \begin{cases} MOD & (MOD == 0) \\ MYD & (MOD > 1 \ \& \ MYD == 0) \\ MOD & (MOD == 1 \ \& \ MYD == 1) \\ NULL & (MOD > 1 \ \& \ MYD > 0) \end{cases} \quad (6)$$

181 The annual MMD dataset is then calculated by averaging the 12 monthly images.

182

183 3.2.2 Landuse data

184 The landuse dataset MCD12Q1 Version 51 (MODIS/Terra+Aqua Land Cover Type Yearly L3 Global 500m SIN
185 Grid V051) in period of 2001-2013 is used to identify the outliers of MMD, while the IGBP (International
186 Geosphere Biosphere Programme) classification is adopted for its wide applications. Due to mismatch in spatial
187 resolutions between MMD and MCD12Q1 datasets, the MCD12Q1 dataset is upscaled to 1km as MMD for outlier
188 identification. It should be noted that for any of the four 500 m pixels in MCD12Q1 classified as water, urban,
189 snow or ice and cropland, the upscaled 1 km pixel will be assigned with a missing value (i.e. -9999) and the
190 corresponding NDVI pixel will be identified as an outlier.

191

192 3.2.3 Weather data

193 Datasets consisting of daily precipitation and air temperature collected at the 59 gauges in the study area are
194 obtained via the China Meteorological Data Sharing Service system
195 (http://data.cma.cn/data/detail/dataCode/SURF_CLI_CHN_MUL_DAY_V3.0/keywords/v3.0.html).

196 The air temperature measurements will be used for dependence analysis later in Section 4.5. The streamflow data
197 provided by Yunnan University will be used for calculating sub-basin scale precipitation based on water balance.
198 The 5 hydrological stations are Gongshan, Liuku, Jiucheng, Gulaohe and Dawanjiang with the drainage area of
199 101146, 106681, 6308, 4185 and 7986 km², respectively. MODIS evapotranspiration (ET) product MOD16
200 (<http://www.nts.gov.cn/project/mod16>) with the spatiotemporal resolution of 1 km/1 weekly will also be
201 used in calculating precipitation based on water balance.

202

203 4 Results and discussion

204 4.1 Model calibration and validation

205 Based on the results of six evaluation metrics for different regression form candidates (Fig. 3a), the 2nd-order
206 polynomial is chosen as the regression model form in this study:

$$p = a NDVI^2 + b NDVI + c \quad (7)$$

207 where p denotes precipitation amount in mm, and a , b and c are regression coefficients. The results of regression
208 coefficients and evaluation metrics are given in Table 1, and the NDVI-precipitation relationships for the study

209 period are demonstrated in Fig. 3b.

210

211 The best performance of the regression model is found within $0.2 < \text{NDVI} < 0.7$ and $400 \text{ mm year}^{-1} < p < 1500$
212 mm year^{-1} . Larger errors are found at pixels with NDVI larger than 0.7 or annual rainfall larger than 1500 mm,
213 implying the water supply is no longer a determinant of vegetation growth as annual rainfall exceeds a certain
214 threshold.

215

216 In general, the RMIs demonstrate better performance than RME, which can be attributable to the less variability
217 of precipitation in a single year than the whole study period. It is also noted that the R^2 values of RMIs for drier
218 years (2003, 2009 and 2011) are less than wetter years, indicating the weaker coupling effect between vegetation
219 growth and precipitation.

220

221 The performance of regression models is assessed under three scenarios as described in Section 2.2. A total of 300
222 tests are conducted and performance metrics (i.e., R , R^2 , E_{RMS} , and E_{MAR}) are calculated accordingly (Fig. 4 and
223 Table 2). The high R values (> 0.85) indicate a strong correlation between NDVI and precipitation independent
224 of sampling method. Also, the regression models demonstrate good performance with R^2 larger than 0.75 and
225 E_{MAR} less than 20%. In addition, the metrics of regression models fluctuate around that of the RME with narrow
226 inter-quartile ranges, indicating the regression models have remarkable consistency with the RME model.

227

228 Scenario a is designed to examine inter-annual stability in the performance of regression models, where the good
229 performance indicates the acceptable ability of the RME model in estimating precipitation during periods when
230 precipitation measurements are not available. Scenarios b and c investigate the impacts of spatial and temporal
231 coverages of measurements, respectively. It is noteworthy that under scenario b better performance in regression
232 models is observed as compared with scenario c, implying greater importance of spatial coverage of measurements
233 in conducting the regressions. In addition, the results of calibration is better than validation as revealed by all
234 metrics criteria as expected. However, the differences between calibration and validation are not significant,
235 implying the consistent performance of regression models under various scenarios.

236

237 The performance of RME is further assessed by comparing the estimates against observations (Fig. 5), and good

238 agreement between estimates and observations is observed. It should be noted the RME shows difficulty in
239 estimating precipitation larger 2000 mm (cf. the dashed line in Fig. 5), implying the limitation of the fusion
240 framework inherited from the oversaturation effect of vegetation index.

241

242 Elevation effect on the relationship between precipitation and NDVI is a concern to appreciate. An overall
243 negative relationship is found between precipitation and elevation for the whole elevation range (i.e., 0–5000 m)
244 with the R^2 value of 0.62 (Fig. 6a), whereas there is only unapparent/weak relationship at different elevation bands
245 (Fig. 6b-f). Given the spatial heterogeneity of orographic effects on precipitation (Brunsdon et al., 2001; Daly et
246 al., 2008) and insufficient data of this study, a more thorough investigation of the relationship between
247 precipitation and elevation needs to be conducted with more information that might be available in the future.
248 Positive precipitation-NDVI relationships are found at different elevation bands (Fig. 7) with the best and worst
249 fitness observed at elevation band 2000–3500 m with the R^2 value of 0.94 and at elevation band 0–2000 m with
250 the R^2 value of 0.62, respectively. By comparing the three regressions at different bands with the global regression,
251 we notice that more significant overestimates of precipitation are observed with the range of lower NDVI values
252 (<0.4) at band 0–2000 m than other three regressions, whereas regression at band >3500 m has an significant
253 overestimation of precipitation than other three regressions for higher NDVI values (>0.5).

254

255 4.2 Spatial characteristics of precipitation

256 The spatial characteristics of precipitation of the study area are investigated with RME for the whole study period
257 (Fig. 8). Annual precipitation in Nu River is observed to decrease from south to north and from west to east with
258 prominent spatial variability. Two "hot-spot" regions, whose annual precipitation exceeds 1500 mm, can be
259 identified in the study areas: one near south border and the other close to southwestern mountain border. The east
260 part of the Nu river basin featuring a dry and warm climate receives an average annual precipitation of 800 mm
261 with large inter-annual variability. A precipitation product (DEMP) based on precipitation-elevation relationship
262 is used to compare with RME. There is no obvious distribution pattern of precipitation (Fig.9a) and a smaller
263 spatial variability compared to RME in the DEM product, indicating the advantage of RME in representing the
264 spatial variability of annual precipitation. And the overall underestimation of precipitation is observed in the
265 DEM product across the whole study area (Fig.9b). In addition, the pixels in Fig.8 with a value out of the valid
266 range (i.e., $400 \text{ mm yr}^{-1} < P < 1500 \text{ mm yr}^{-1}$) may have relatively large error as discussed in section 4.1. As there

267 is no justifiable methods for such correction and given the limited fraction of invalid pixels (10% in the whole
268 study area and 7% in the Nu River basin), the figure can be used to demonstrate a full picture of the spatial
269 precipitation pattern in the study area, but we note those pixels are of large uncertainties and should be interpreted
270 with caution.

271

272 4.3 Model performance comparison

273 The performance between IDW approach, TRMM product and the fusion framework is compared in this section.
274 IDW is one of the most popular methods for spatial interpolation of rainfall due to its easy implementation and
275 flexibility in incorporating other auxiliary information (e.g., elevation). In general, the IDW approach is unable to
276 demonstrate the high spatial variability though it can capture the general spatial distribution of whole basin (Fig.
277 10a) as TRMM (Fig. 10b). Due to the coarse spatial resolution, TRMM cannot capture the high variability in the
278 river valley where the elevation varies significantly. Although large rainfall (>1800mm) is observed in both our
279 and TRMM products in the southwest of the study area region, our product gives lower rainfall compared to
280 TRMM. As discussed above, the regression model tends to underestimate rainfall as the annual rainfall exceeds a
281 certain threshold because the water supply is no longer a determinant of vegetation growth.

282

283 To demonstrate the advantage of the fusion framework, a cross-validation is conducted against the randomly
284 sampled gauge observations by varying the number of samples (1 - 40). The cross-validation shows higher E_{RMS}
285 for the IDW approach, followed by TMMM and RME (Fig. 11a). A higher mean E_{MR} of 15% is observed for
286 TRMM than IDW (8%) and RME (5%) while the difference in E_{MAR} are minimal between TRMM and IDW. The
287 results indicate an overestimated precipitation by TRMM as compared to gauge observations. Table 3 summarizes
288 the maximum, minimum and mean values of each method and shows the relative difference between RME and
289 other two methods. On average, E_{RMS} of RME is smaller than that of IDW and TRMM by 20.4% and 17.4%,
290 respectively. In general, the fusion framework demonstrates better performance than the other approaches.

291

292 To further evaluate the performance of RME, the annual averages of precipitation of five hydrological stations
293 (Fig. 12a) and whole basin estimated by the three approaches (IDW, RME and TRMM) are compared. At the
294 whole basin scale, the estimate by RME is 5.2% higher than that of IDW while 7.9% lower than TRMM. Although
295 the difference between the three approaches is minimal at the basin scale, the difference at the sub-basin scale is

296 remarkable. In the upstream region (i.e., Gongshan sub-basin) located in Tibet Plateau, TRMM overestimates
297 precipitation by 13.2% while IDW underestimates by 7.6% as compared with RME. In the other four downstream
298 sub-basins, estimates by RME are larger than those by IDW and TRMM. In general, in the midstream and
299 downstream regions with large variability in terrain height, RME gives larger estimates of precipitation than IDW
300 and TRMM.

301

302 To validate the accuracy of different precipitation estimates, we utilize MODIS evapotranspiration products
303 MOD16 to calculate water budget based precipitation (i.e. ET+R) and to compare it with 5 products including
304 RME, BandP (rainfall based on precipitation-NDVI relationship with consideration elevation band), DEMP,
305 TRMM, IDW (Fig.12b). Although all the 5 products underestimate the sub-basin scale precipitation, RME and
306 BandP give the closest estimates to the water budget based precipitation, indicating the effectiveness of
307 precipitation-NDVI relationship in precipitation remapping.

308

309 We also compared our products with the Multi-Source Weighted-Ensemble Precipitation (MSWEP) product. The
310 dataset takes the advantage of a wide range of data sources, including gauges, satellites, and atmospheric
311 reanalysis models, to obtain the best possible precipitation estimates at the global scale with a high 3-hourly
312 temporal and 0.25 ° spatial resolution (Beck et al., 2016). Comparison in the annual mean precipitation between
313 the gauge measurements and predictions by the MSWEP and TRMM product (Fig. 13) shows acceptable
314 performance of both MSWEP and TRMM in predicting the precipitation with an overall overestimation. The
315 RMSE values for MSWEP, TRMM and RME are 241 mm, 196 mm, and 174 mm, respectively, indicating that
316 RME gives the best prediction among the three products. The possible reason why MSWEP shows no superiority
317 over TRMM in predicting annual precipitation is that very few gauges are available in this region that might limit
318 the applicability of MSWEP methodology. However, the MSWEP methodology does provide insights into the
319 production of high temporal resolution (3-hourly) rainfall, which we believe will be helpful to our future work.

320

321 **4.4 influence of different vegetation index**

322 Considering the possible degradation in model performance caused by oversaturation of NDVI in high biomass
323 areas, another vegetation indicator, Enhanced Vegetation Index (EVI), is suggested as an alternative for estimating
324 vegetation growth (Matsushita et al., 2007; Liao et al., 2015). As such, we also test the fusion framework with

325 EVI in addition to NDVI and the results are assessed against the gauge observations.

326

327 Based on the chosen metrics, EVI is found to outperform NDVI with better regression quality (Table 4): EVI-
328 based regression model gives higher R^2 , smaller E_{RMS} and E_{MAR} compared to the NDVI-based model. Also,
329 remarkable difference is observed in the precipitation estimates based on the two vegetation indices (Fig. 14). It
330 is noted that the curvature of EVI-based model is larger than NDVI-based model, suggesting higher sensitivity of
331 EVI-based model in humid environment. Although the EVI-based model demonstrates better performance than
332 the NDVI-based one, it should be noted that NDVI is the most popular vegetation index used in operational
333 applications among the available vegetation index products. Besides, NDVI has a relative longer temporal
334 coverage compared to other vegetation index products. For instance, the AVHRR (Advanced Very High
335 Resolution Radiometer) NDVI data are available since 1982 with a global coverage. As such, under scenarios
336 when EVI is unavailable, NDVI is a satisfactory index that can be used in the fusion framework.

337

338 **4.5 Influence of other ambient determinants**

339 One major assumption of the proposed framework is that precipitation is the only determinant of vegetation
340 growth and thus NDVI is regarded as a proxy for precipitation. However, other ambient factors, such as soil
341 properties, solar radiation, air temperature, elevation, etc., may significantly influence the vegetation growth as
342 well as NDVI values. Considering the data availability of various ambient factors, air temperature and elevation,
343 in addition to NDVI, are adopted as extra determinants to establish the regression models, which are thus termed
344 as RME+T and RME+H for air temperature and elevation, respectively. We note that for simplicity, the extra
345 determinants are assumed to have linear relationship with precipitation.

346

347 The difference in R^2 , E_{RMS} , and E_{MAR} between the three models are minimal and the regression coefficients of the
348 three models are very close to each other (Table 5). The negative regression coefficient of temperature in RME+T
349 indicates inconsistent trends between precipitation and temperature. Since the temperature decreases with the
350 increase in elevation, RME+T and RME+H essentially provides consistent estimates of precipitation which is also
351 clearly shown in Fig. 15. It is also noted the added information by extra determinants (i.e., air temperature and
352 elevation) is in fact minimal. Overall there is little difference between RME and other two products. As such, we
353 consider the RME-only based vegetation index as a simple and efficient model for precipitation estimation.

354

355 **5 Conclusion**

356 In this study, a satellite-gauge-vegetation fusion framework has been developed for estimating the precipitation
357 in mountainous areas by establishing regression relationship between gauge-based precipitation observations and
358 satellite-based vegetation dataset. The fusion framework was then applied in the Nu River basin of Southwest
359 China for estimating precipitation between 2001 and 2012.

360

361 The fusion framework for the Nu River basin adopted a second order polynomial form and demonstrated
362 promising ability in capturing the high spatial variability of precipitation in the river valley. Six evaluation metrics,
363 including R , R^2 , E_{RMS} , E_{MR} and E_{MAR} , indicated good performance of the fusion framework in precipitation
364 estimation. The performance of the fusion framework was also compared with the IDW approach and TRMM
365 product and the comparison results indicated that the fusion framework generally outperformed other approaches
366 in estimating precipitation in mountainous areas. On average, the E_{RMS} of the fusion framework is 20.4%, 17.4%
367 smaller than that of IDW and TRMM, respectively. E_{MR} of the fusion framework is 1.2%, 71.5% smaller than that
368 of IDW and TRMM. E_{MAR} the fusion framework is 18.9%, 28.3% smaller than that of IDW and TRMM.

369

370 The success of application of the fusion framework in the Nu River sheds light on the precipitation estimation in
371 mountainous areas by using multi-source datasets. However, this framework does have certain limitations that are
372 important to appreciate. First, the framework is applied only in the Nu River basin. More mountainous areas under
373 different climates need to be examined to further test the robustness of this framework. In addition, although the
374 RME model can utilize the full knowledge of precipitation in the entire study period compared with RMI models,
375 the difference in the coefficients suggests apparent inter-annual variability of precipitation that should be
376 considered when applying these models. Given the duration of study period and purpose, we suggest the RME
377 model be used for long-term climatology identification while RMI models for inter-annual variability examination.
378 Also, to fully verify the theoretical basis of this framework that vegetation actively interacts with precipitation in
379 mountainous areas, future work is required to refine the spatiotemporal resolution of this study to enable better
380 scrutiny into vegetation-precipitation interactions at sub-monthly scales across more detailed vegetation species.

381 **Acknowledgments**

382 The study is supported by NSFC under grant U1202231, 51679119 and 91647107, National Key Technology
383 Support Program under grant 2011BAC09B07-3 and by China Postdoctoral Science Foundation under grant
384 2015T80093. The authors thank China Meteorological Administration, Yunnan University, MODIS NDVI,
385 Tropical Rainfall Measuring Mission (TRMM) and the Shuttle Radar Topography Mission (SRTM) for providing
386 the data used in this study.

387

388 **Appendix: Merging of NDVI datasets**

389 The merging of NDVI datasets improves the accuracy as expected (Fig. A1), the monthly error rates (i.e., the ratio
390 of the pixel which quality value is over 1) of MOD and MMD are generally reduced with an average of 5% and
391 over 20% in several months. Fig.A2 shows that the accuracy of MMD is significantly improved in a ridge area
392 covering 23 °10' N–23 °40' N and 98 °30' E–99 ° E. Fig. A2b shows NDVI value near right and left boundary is
393 underestimated by MOD. Fig.A2c shows NDVI value in the middle boundary is underestimated by MYD. The
394 underestimates in both products near the boundary of MOD and MYD are amended (Fig. A2a). Fig.A3 shows the
395 three NDVI series for one rain gauge. Comparing with MOD series, the improved accuracy in MMD is mainly
396 observed in the wet season (from May to October), when the NDVI values could be often underestimated due to
397 the overcasts.

398 **References**

- 399 Akbari, A., Abu Samah, A. and Othman, F.: Integration of SRTM and TRMM data into the GIS-based hydrological
400 model for the purpose of flood modelling, *Hydrol Earth Syst Sci Discuss*, 2012, 4747–4775,
401 doi:10.5194/hessd-9-4747-2012, 2012.
- 402 Borges, P. de A., Franke, J., Anunciação, Y. M. T. da, Weiss, H. and Bernhofer, C.: Comparison of spatial
403 interpolation methods for the estimation of precipitation distribution in Distrito Federal, Brazil, *Theor. Appl.*
404 *Climatol.*, 123(1–2), 335–348, doi:10.1007/s00704-014-1359-9, 2016.
- 405 Beck, H.E., A.I.J.M. van Dijk, V. Levizzani, J. Schellekens, D.G. Miralles, B. Martens, A. de Roo (2016):
406 MSWEP: 3-hourly 0.25 ° global gridded precipitation (1979–2015) by merging gauge, satellite, and
407 reanalysis data, *Hydrology and Earth System Sciences Discussions*, doi:10.5194/hess-2016–236.
- 408 Brunson, C., McClatchey, J. and Unwin, D. J.: Spatial variations in the average rainfall-altitude relationship in
409 Great Britain: an approach using geographically weighted regression, *Int. J. Climatol.*, 21, 455–466,
410 doi:10.1002/joc.614, 2001.
- 411 Campo-Bescós, M. A., Muñoz-Carpena, R., Southworth, J., Zhu, L., Waylen, P. R. and Bunting, E.: Combined

412 Spatial and Temporal Effects of Environmental Controls on Long-Term Monthly NDVI in the Southern
413 Africa Savanna, *Remote Sens.*, 5(12), 6513–6538, doi:10.3390/rs5126513, 2013.

414 Chen, F. and Li, X.: Evaluation of IMERG and TRMM 3B43 Monthly Precipitation Products over Mainland China,
415 *Remote Sens.*, 8(6), 472, doi:10.3390/rs8060472, 2016.

416 Chen, F., Liu, Y., Liu, Q. and Li, X.: Spatial downscaling of TRMM 3B43 precipitation considering spatial
417 heterogeneity, *Int. J. Remote Sens.*, 35(9), 3074–3093, doi:10.1080/01431161.2014.902550, 2014.

418 Chen, J., Yong, B., Ren, L., Wang, W., Chen, B., Lin, J., Yu, Z. and Li, N.: Using a Kalman Filter to Assimilate
419 TRMM-Based Real-Time Satellite Precipitation Estimates over Jinghe Basin, China, *Remote Sens.*, 8(11),
420 899, doi:10.3390/rs8110899, 2016.

421 Council, N. R.: Assessment of the Benefits of Extending the Tropical Rainfall Measuring Mission: A Perspective
422 from the Research and Operations Communities, Interim Report. [online] Available from:
423 [https://www.nap.edu/catalog/11195/assessment-of-the-benefits-of-extending-the-tropical-rainfall-](https://www.nap.edu/catalog/11195/assessment-of-the-benefits-of-extending-the-tropical-rainfall-measuring-mission)
424 [measuring-mission](https://www.nap.edu/catalog/11195/assessment-of-the-benefits-of-extending-the-tropical-rainfall-measuring-mission) (Accessed 18 November 2016), 2005.

425 Daly, C., Halbleib, M., Smith, J. I., Gibson, W. P., Doggett, M. K., Taylor, G. H., Curtis, J. and Pasteris, P. P.:
426 Physiographically sensitive mapping of climatological temperature and precipitation across the
427 conterminous United States, *Int. J. Climatol.*, 28, 2031–2064, doi:10.1002/joc.1688, 2008.

428 Duan, Z. and Bastiaanssen, W. G. M.: First results from Version 7 TRMM 3B43 precipitation product in
429 combination with a new downscaling–calibration procedure, *Remote Sens. Environ.*, 131, 1–13,
430 doi:10.1016/j.rse.2012.12.002, 2013.

431 Huffman, G. J., Adler, R. F., Arkin, P., Chang, A., Ferraro, R., Gruber, A., Janowiak, J., McNab, A., Rudolf, B.
432 and Schneider, U.: The Global Precipitation Climatology Project (GPCP) Combined Precipitation Dataset,
433 *Bull. Am. Meteorol. Soc.*, 78(1), 5–20, doi:10.1175/1520-0477(1997)078<0005:TGPCPG>2.0.CO;2, 1997.

434 Immerzeel, W. W., Rutton, M. M. and Droogers, P.: Spatial downscaling of TRMM precipitation using vegetative
435 response on the Iberian Peninsula, *Remote Sens. Environ.*, 113(2), 362–370, doi:10.1016/j.rse.2008.10.004,
436 2009.

437 Jacquin, A. P. and Soto-Sandoval, J. C.: Interpolation of monthly precipitation amounts in mountainous
438 catchments with sparse precipitation networks, *Chil. J. Agric. Res.*, 73(4), 406–413, doi:10.4067/S0718-
439 58392013000400012, 2013.

440 Jia, S., Zhu, W., Lü, A. and Yan, T.: A statistical spatial downscaling algorithm of TRMM precipitation based on
441 NDVI and DEM in the Qaidam Basin of China, *Remote Sens. Environ.*, 115(12), 3069–3079,
442 doi:10.1016/j.rse.2011.06.009, 2011.

443 Jing, W., Yang, Y., Yue, X. and Zhao, X.: A Spatial Downscaling Algorithm for Satellite-Based Precipitation over
444 the Tibetan Plateau Based on NDVI, DEM, and Land Surface Temperature, *Remote Sens.*, 8(8), 655,
445 doi:10.3390/rs8080655, 2016.

446 Joyce, R. J., Janowiak, J. E., Arkin, P. A. and Xie, P.: CMORPH: A Method that Produces Global Precipitation
447 Estimates from Passive Microwave and Infrared Data at High Spatial and Temporal Resolution, *J.*
448 *Hydrometeorol.*, 5(3), 487–503, doi:10.1175/1525-7541(2004)005<0487:CAMTPG>2.0.CO;2, 2004.

449 Kariyeva, J. and Van Leeuwen, W. J. D.: Environmental Drivers of NDVI-Based Vegetation Phenology in Central
450 Asia, *Remote Sens.*, 3(2), 203–246, doi:10.3390/rs3020203, 2011.

451 Kneis, D., Chatterjee, C. and Singh, R.: Evaluation of TRMM rainfall estimates over a large Indian river basin
452 (Mahanadi), *Hydrol Earth Syst Sci*, 18(7), 2493–2502, doi:10.5194/hess-18-2493-2014, 2014.

453 Krakauer, N. Y., Pradhanang, S. M., Lakhankar, T. and Jha, A. K.: Evaluating Satellite Products for Precipitation
454 Estimation in Mountain Regions: A Case Study for Nepal, *Remote Sens.*, 5(8), 4107–4123,
455 doi:10.3390/rs5084107, 2013.

456 Li, B., Tao, S. and Dawson, R. W.: Relations between AVHRR NDVI and ecoclimatic parameters in China, *Int. J.*
457 *Remote Sens.*, 23(5), 989–999, doi:10.1080/014311602753474192, 2002.

458 Li, D., Ding, X. and Wu, J.: Simulating the regional water balance through hydrological model based on TRMM
459 satellite rainfall data, *Hydrol Earth Syst Sci Discuss*, 2015, 2497–2525, doi:10.5194/hessd-12-2497-2015,
460 2015.

461 Li, H., Calder, C. A. and Cressie, N.: Beyond Moran’s I: Testing for Spatial Dependence Based on the Spatial
462 Autoregressive Model, *Geogr. Anal.*, 39(4), 357–375, doi:10.1111/j.1538-4632.2007.00708.x, 2007.

463 Li, Z. and Guo, X.: Detecting Climate Effects on Vegetation in Northern Mixed Prairie Using NOAA AVHRR 1-
464 km Time-Series NDVI Data, *Remote Sens.*, 4(1), 120–134, doi:10.3390/rs4010120, 2012.

465 Liao, Z., He, B. and Quan, X.: Modified enhanced vegetation index for reducing topographic effects, *J. Appl.*
466 *Remote Sens.*, 9(1), 096068–096068, doi:10.1117/1.JRS.9.096068, 2015.

467 Lloyd, C. D.: Assessing the effect of integrating elevation data into the estimation of monthly precipitation in
468 Great Britain, *J. Hydrol.*, 308(1–4), 128–150, doi:10.1016/j.jhydrol.2004.10.026, 2005.

469 Mahmud, M. R., Numata, S., Matsuyama, H., Hosaka, T. and Hashim, M.: Assessment of Effective Seasonal
470 Downscaling of TRMM Precipitation Data in Peninsular Malaysia, *Remote Sens.*, 7(4), 4092–4111,
471 doi:10.3390/rs70404092, 2015.

472 Mair, A. and Fares, A.: Comparison of Rainfall Interpolation Methods in a Mountainous Region of a Tropical
473 Island, *J. Hydrol. Eng.*, 16(4), 371–383, doi:10.1061/(ASCE)HE.1943-5584.0000330, 2011.

474 Marquínez, J., Lastra, J. and García, P.: Estimation models for precipitation in mountainous regions: the use of
475 GIS and multivariate analysis, *J. Hydrol.*, 270(1–2), 1–11, doi:10.1016/S0022-1694(02)00110-5, 2003.

476 Matsushita, B., Yang, W., Chen, J., Onda, Y. and Qiu, G.: Sensitivity of the Enhanced Vegetation Index (EVI) and
477 Normalized Difference Vegetation Index (NDVI) to Topographic Effects: A Case Study in High-density
478 Cypress Forest, *Sensors*, 7(11), 2636–2651, doi:10.3390/s7112636, 2007.

479 Mourre, L., Condom, T., Junquas, C., Lebel, T., E. Sicart, J., Figueroa, R. and Cochachin, A.: Spatio-temporal
480 assessment of WRF, TRMM and in situ precipitation data in a tropical mountain environment
481 (Cordillera Blanca, Peru), *Hydrol Earth Syst Sci*, 20(1), 125–141, doi:10.5194/hess-20-125-2016, 2016.

482 Phillips, D. L., Dolph, J. and Marks, D.: A comparison of geostatistical procedures for spatial analysis of
483 precipitation in mountainous terrain, *Agric. For. Meteorol.*, 58(1), 119–141, doi:10.1016/0168-
484 1923(92)90114-J, 1992.

485 Schamm, K., Ziese, M., Becker, A., Finger, P., Meyer-Christoffer, A., Schneider, U., Schröder, M. and Stender, P.:
486 Global gridded precipitation over land: a description of the new GPCC First Guess Daily product, *Earth*
487 *Syst. Sci. Data*, 6(1), 49–60, doi:10.5194/essd-6-49-2014, 2014.

488 Song, J., Xia, J., Zhang, L., Wang, Z.-H., Wan, H. and She, D.: Streamflow prediction in ungauged basins by
489 regressive regionalization: a case study in Huai River Basin, China, *Hydrol. Res.*, nh2015155,
490 doi:10.2166/nh.2015.155, 2015.

491 Sun, J., Cheng, G., Li, W., Sha, Y. and Yang, Y.: On the Variation of NDVI with the Principal Climatic Elements
492 in the Tibetan Plateau, *Remote Sens.*, 5(4), 1894–1911, doi:10.3390/rs5041894, 2013.

493 Wang, S., Huang, G. H., Lin, Q. G., Li, Z., Zhang, H. and Fan, Y. R.: Comparison of interpolation methods for
494 estimating spatial distribution of precipitation in Ontario, Canada, *Int. J. Climatol.*, 14(34), 3745–3751,
495 doi:10.1002/joc.3941, 2014.

496 Woldemeskel, F. M., Sivakumar, B. and Sharma, A.: Merging gauge and satellite rainfall with specification of
497 associated uncertainty across Australia, *J. Hydrol.*, 499, 167–176, doi:10.1016/j.jhydrol.2013.06.039, 2013.

498 Wong, J. S., Razavi, S., Bonsal, B. R., Wheatler, H. S. and Asong, Z. E.: Evaluation of various daily precipitation
499 products for large-scale hydro-climatic applications over Canada, *Hydrol Earth Syst Sci Discuss*, 2016, 1–

500 51, doi:10.5194/hess-2016-511, 2016.

501 Worqlul, A. W., Collick, A. S., Tilahun, S. A., Langan, S., Rientjes, T. H. M. and Steenhuis, T. S.: Comparing
502 TRMM 3B42, CFSR and ground-based rainfall estimates as input for hydrological models, in data scarce
503 regions: the Upper Blue Nile Basin, Ethiopia, Hydrol Earth Syst Sci Discuss, 2015, 2081–2112,
504 doi:10.5194/hessd-12-2081-2015, 2015.

505 Xu, S., Wu, C., Wang, L., Gonsamo, A., Shen, Y. and Niu, Z.: A new satellite-based monthly precipitation
506 downscaling algorithm with non-stationary relationship between precipitation and land surface
507 characteristics, Remote Sens. Environ., 162, 119–140, doi:10.1016/j.rse.2015.02.024, 2015.

508 Zhou, L., Chen, Y., Liang, N. and Ni, Y.: Daily rainfall model to merge TRMM and ground based observations
509 for rainfall estimations, in 2016 IEEE International Geoscience and Remote Sensing Symposium (IGARSS),
510 pp. 601–604., 2016.

511

512

513

514

515

516

517

518

519

520

521

522

523

524

525

526

527

528

529

530

531

532

533 **Table 1** Regression model performance and regression coefficients.

| Year | Mean (mm) | R^2 | E_{RMS} (mm) | E_{MAR} (%) | a | b | c |
|------|--------------|-------|-------------------|------------------|--------|---------|-------|
| 2001 | 961 | 0.91 | 138 | 10.6 | 3038.1 | -345.3 | 359.8 |
| 2002 | 887 | 0.90 | 119 | 10.2 | 1354.7 | 687.5 | 212.0 |
| 2003 | 828 | 0.75 | 155 | 14.0 | 1700.2 | -115.5 | 472.7 |
| 2004 | 1018 | 0.89 | 171 | 12.4 | 3784.3 | -1047.7 | 517.4 |
| 2005 | 810 | 0.93 | 97 | 9.5 | 2465.4 | -265.0 | 363.2 |
| 2006 | 737 | 0.88 | 122 | 11.4 | 2065.2 | -112.2 | 287.5 |
| 2007 | 928 | 0.84 | 184 | 14.6 | 2306.9 | 53.5 | 286.4 |
| 2008 | 960 | 0.91 | 121 | 9.4 | 2504.0 | -258.1 | 433.5 |
| 2009 | 726 | 0.89 | 119 | 13.2 | 2091.3 | -168.0 | 294.5 |
| 2010 | 937 | 0.94 | 124 | 9.1 | 4094.8 | -1293.3 | 512.6 |
| 2011 | 824 | 0.84 | 167 | 14.2 | 4697.8 | -2613.7 | 792.7 |
| 2012 | 791 | 0.89 | 114 | 10.6 | 1966.4 | 3.5 | 308.1 |
| RME | 848 | 0.83 | 174 | 15.2 | 2670.4 | -471.2 | 409.2 |

534

535

536 **Table 2** Statistics of regression models for validation and calibration under three scenarios.

| Scenario | Statistics | Calibration | | | | Validation | | |
|----------|------------|-------------|-------|-------------------|------------------|------------|-------------------|------------------|
| | | R | R^2 | E_{RMS} (mm) | E_{MAR} (%) | R | E_{RMS} (mm) | E_{MAR} (%) |
| a | mean | 0.91 | 0.83 | 175 | 16.6 | 0.91 | 173.9 | 16.8 |
| | max | 0.92 | 0.85 | 186.2 | 17.8 | 0.94 | 211.8 | 19.9 |
| | min | 0.9 | 0.81 | 161.1 | 15.7 | 0.88 | 141 | 13.2 |
| b | mean | 0.92 | 0.84 | 166.6 | 15.8 | 0.91 | 186.1 | 17.8 |
| | max | 0.94 | 0.89 | 207 | 19.7 | 0.95 | 229.7 | 23.3 |
| | min | 0.89 | 0.8 | 126.2 | 12.8 | 0.89 | 148.6 | 12.9 |
| c | mean | 0.91 | 0.82 | 172.7 | 16.5 | 0.91 | 180.8 | 17.3 |
| | max | 0.95 | 0.91 | 207.9 | 19.1 | 0.94 | 204.8 | 24.4 |
| | min | 0.85 | 0.73 | 144.6 | 13.9 | 0.85 | 143.4 | 13.9 |

537

538

539

540

541

542

543

544 **Table 3** Performance comparison between IDW, RME and TRMM

| Method | Statistics | ERMS (mm) | EMR | EMAR |
|-----------------|------------|-----------|-------|-------|
| IDW | max | 273 | 0.1 | 0.26 |
| | min | 249 | 0.08 | 0.23 |
| | mean | 223 | 0.05 | 0.21 |
| TRMM | max | 220 | 0.17 | 0.24 |
| | min | 213 | 0.16 | 0.23 |
| | mean | 203 | 0.15 | 0.22 |
| RME | max | 183 | 0.07 | 0.18 |
| | min | 177 | 0.05 | 0.17 |
| | mean | 168 | 0.04 | 0.16 |
| RME-IDW (%) | max | -32.9 | -33 | -30.5 |
| | min | -26.3 | -9.8 | -21.4 |
| | mean | -20.4 | -1.2 | -18.9 |
| RME-TRMM (%) | max | -16.8 | -59.5 | -23.8 |
| | min | -16.6 | -66 | -25.9 |
| | mean | -17.4 | -71.5 | -28.3 |

545

546 **Table 4** Regression model performance and coefficients of regression

| | R^2 | ERMS (mm) | EMAR (%) | a | b | c |
|------|-------|--------------|-------------|--------|--------|-------|
| NDVI | 0.83 | 174.7 | 14.8 | 2670.4 | -471.2 | 409.2 |
| EVI | 0.87 | 143.8 | 12.4 | 5129.6 | 702.5 | 254.7 |

547

548

549 **Table 5** Results of two regression models established with extra independent variables: RME+T for
550 temperature, RME+H for elevation

| Model | R^2 | ERMS (mm) | EMAR (%) | a | b | c | Extra b |
|-------|-------|--------------|-------------|--------|--------|-------|-----------|
| RME | 0.83 | 174.7 | 15 | 2670.4 | -471.2 | 409.2 | -- |
| RME+T | 0.84 | 172.6 | 15 | 2728.8 | -496 | 407.3 | -0.2 |
| RME+H | 0.84 | 172.6 | 15 | 2838.4 | -638.7 | 492.9 | -0.02 |

551

552

553

554

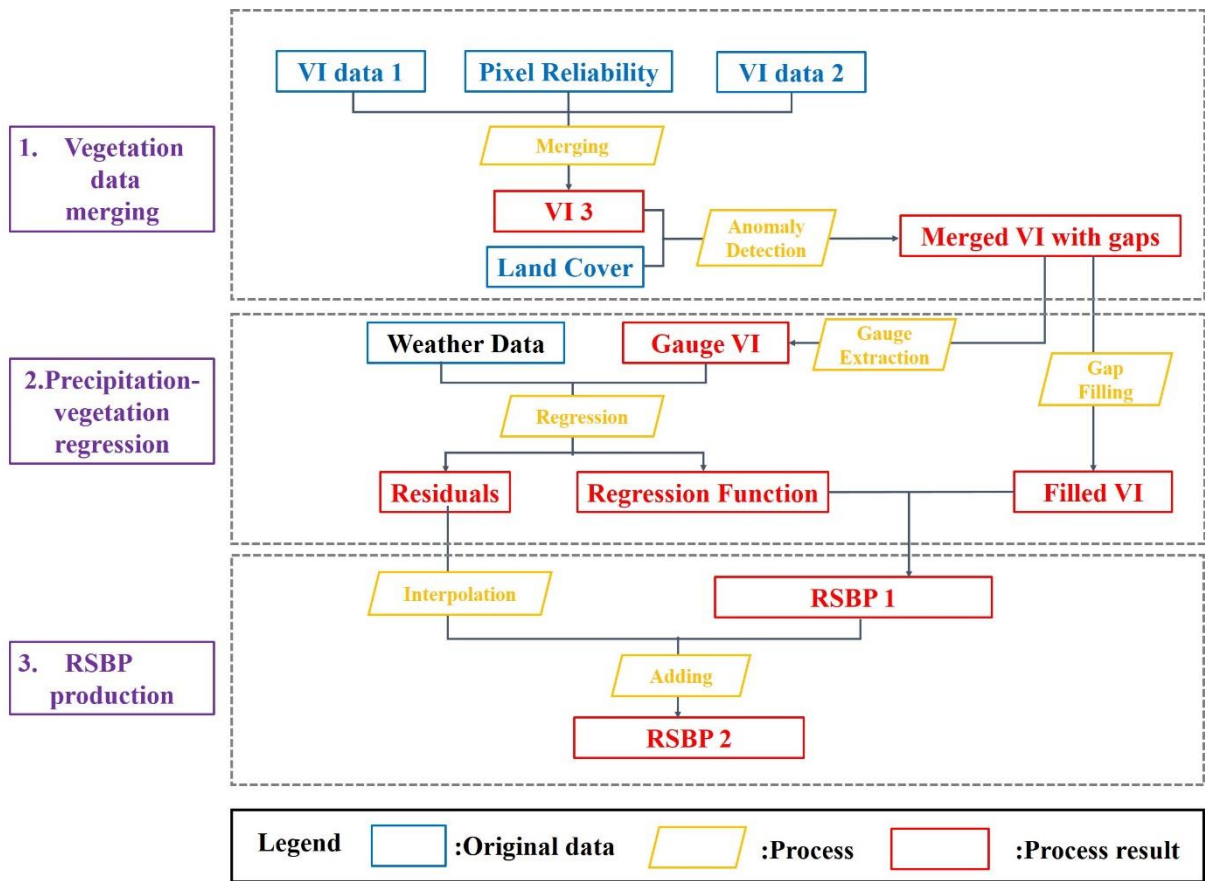


Figure 1 Flow chart of the satellite-gauge-vegetation fusion framework development.

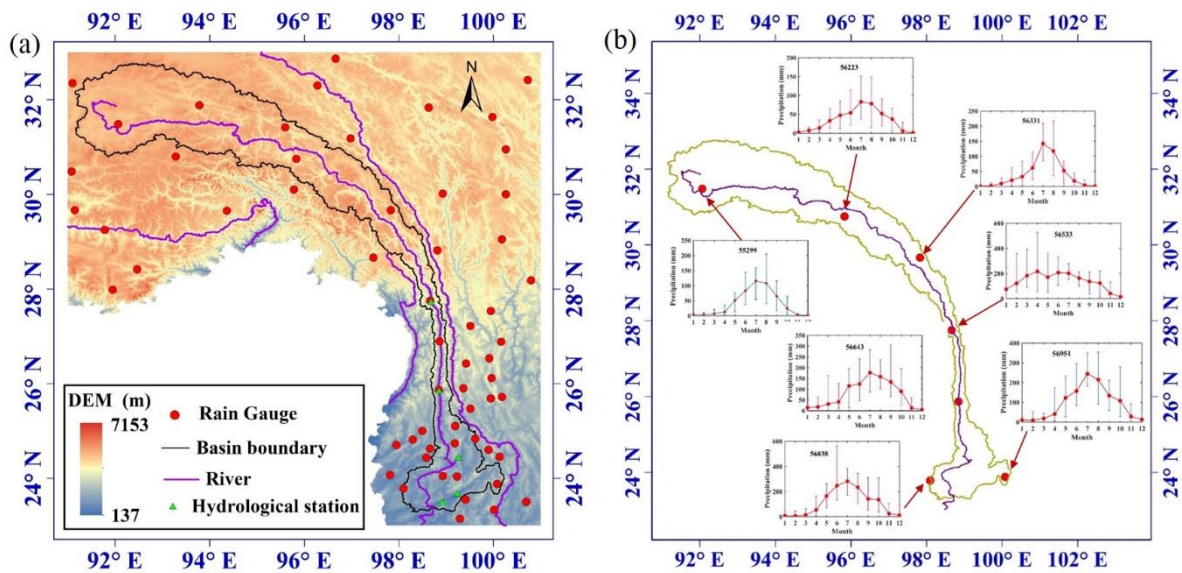
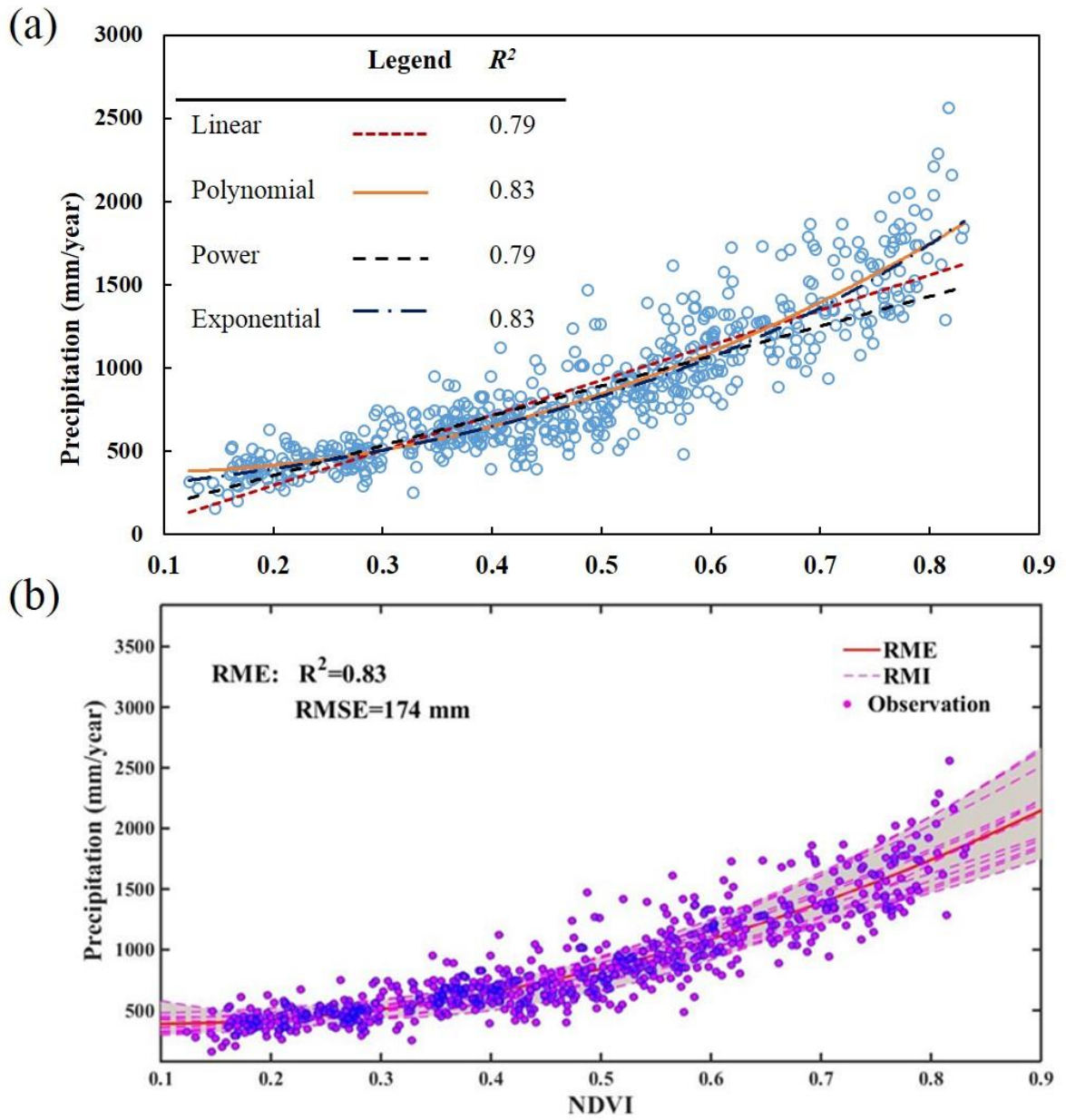


Figure 2 (a) Terrain map of the study area (the Nu-Salween basin and its adjacent areas). (b) The distribution of rainfall during the year across the Nu River.

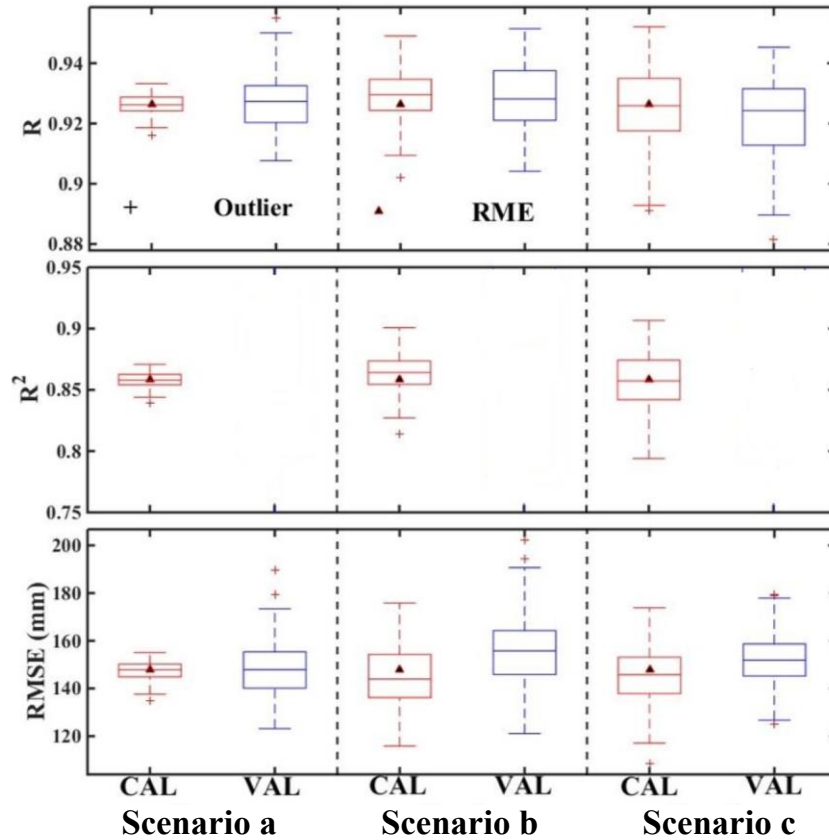


564

565 **Figure 3** (a) Different regression form between annual precipitation and NDVI; (b) The NDVI-precipitation
 566 relationships for RME and RMI

567

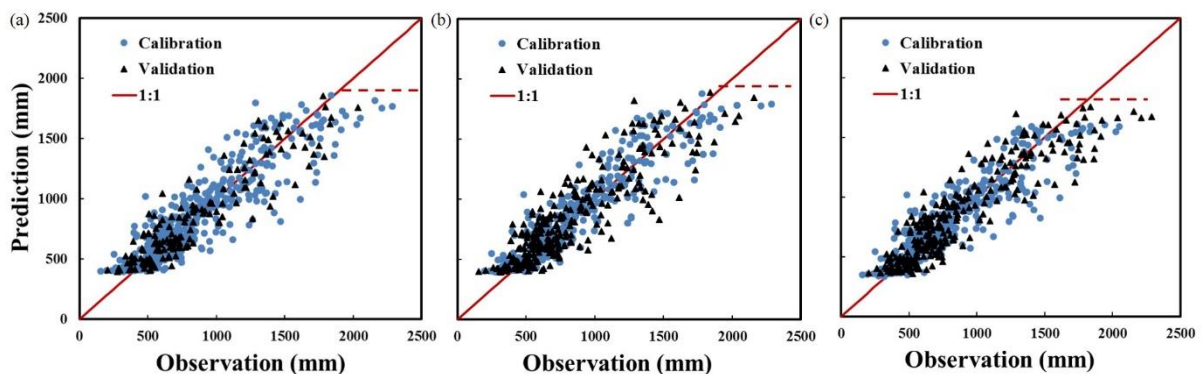
568



569

570 **Figure 4** Box plots of R , R^2 , E_{RMS} of RME model under three scenarios: a) fully random; b) all gauges, partial
 571 period; and c) partial gauges, entire period. Details of the three scenarios refer to Section 2.2. The triangle marker
 572 corresponding the value (R , R^2 , $RMSE$) of RME model. Plus sign represent the outlier of the sample used to drawn
 573 box diagram which value is out of the range from $(Q1-1.5IQR)$ to $(Q3+1.5IQR)$. $Q1$ and $Q3$ represent the lower
 574 and upper quartile, $IQR=Q3-Q1$.

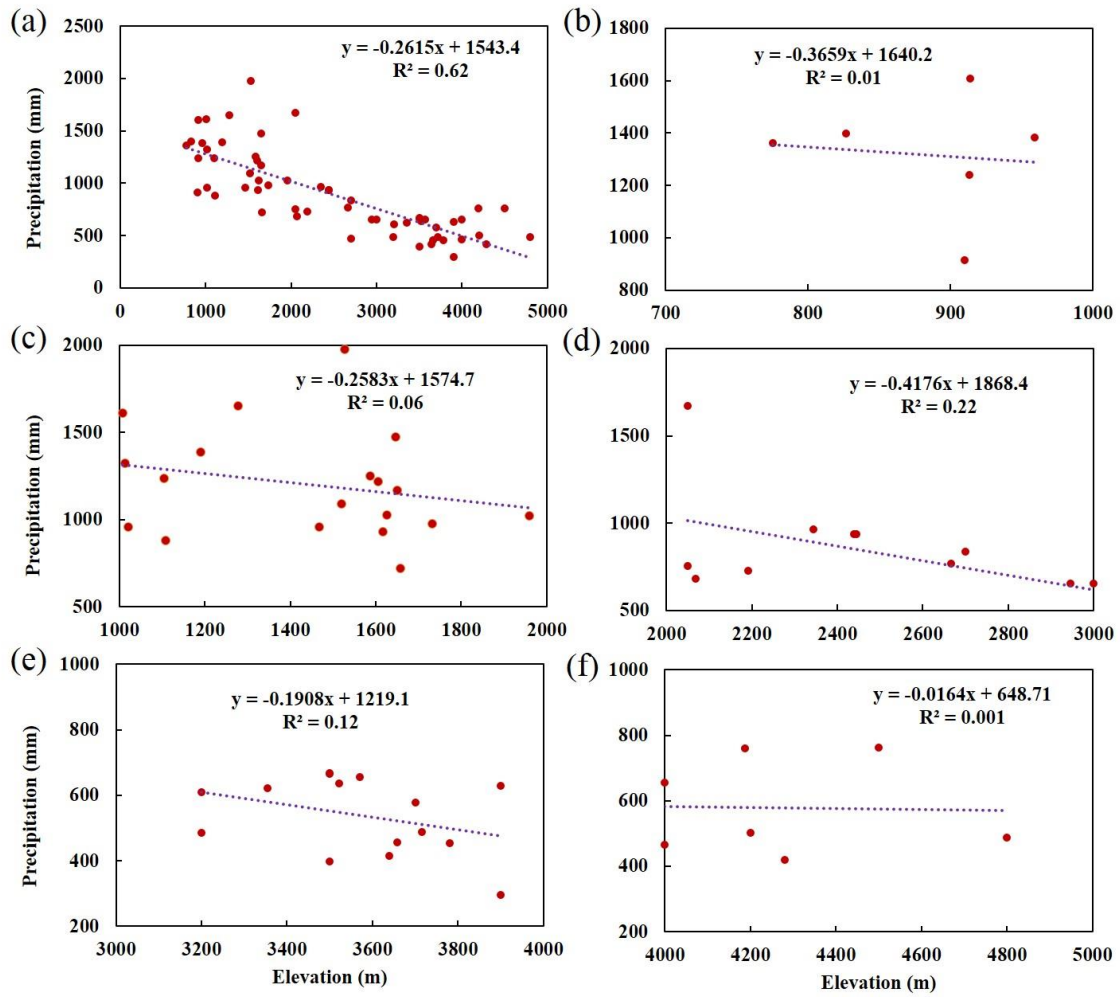
575



576

577 **Figure 5** Comparison in annual precipitation between the gauged measurements and predictions by the
 578 regression model for scenario a) fully random; b) all gauges, partial period; and c) partial gauges, entire period.
 579 Details of the three scenarios refer to Section 2.2.

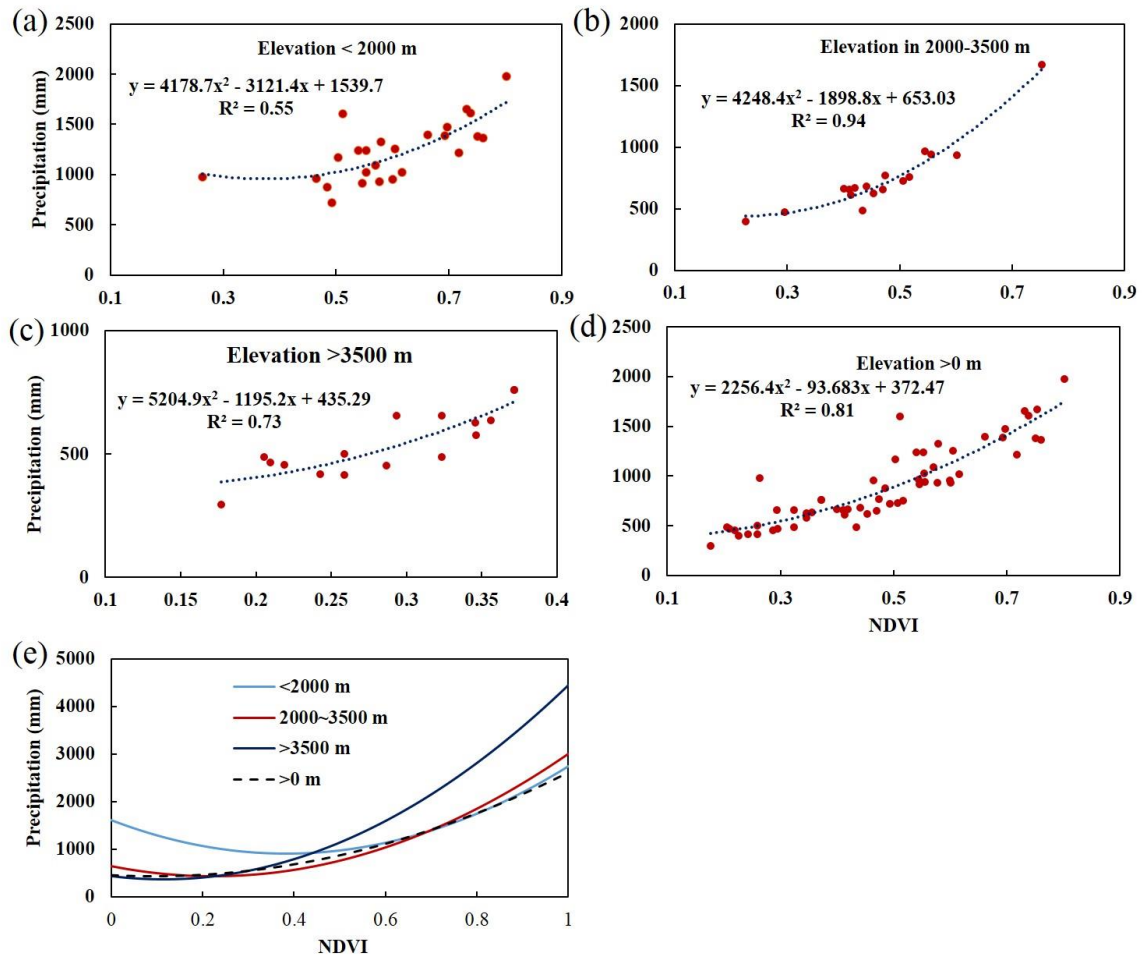
580



582

583 **Figure 6** The relationship between mean annual precipitation and elevation at different elevation bands, (a) whole
 584 elevation bands; (b) elevation band :<1000 m; (c) band:1000~2000 m; (d) band: 2000~3000 m; (e)
 585 band :3000~4000 m; (f) band: >4000 m.

586



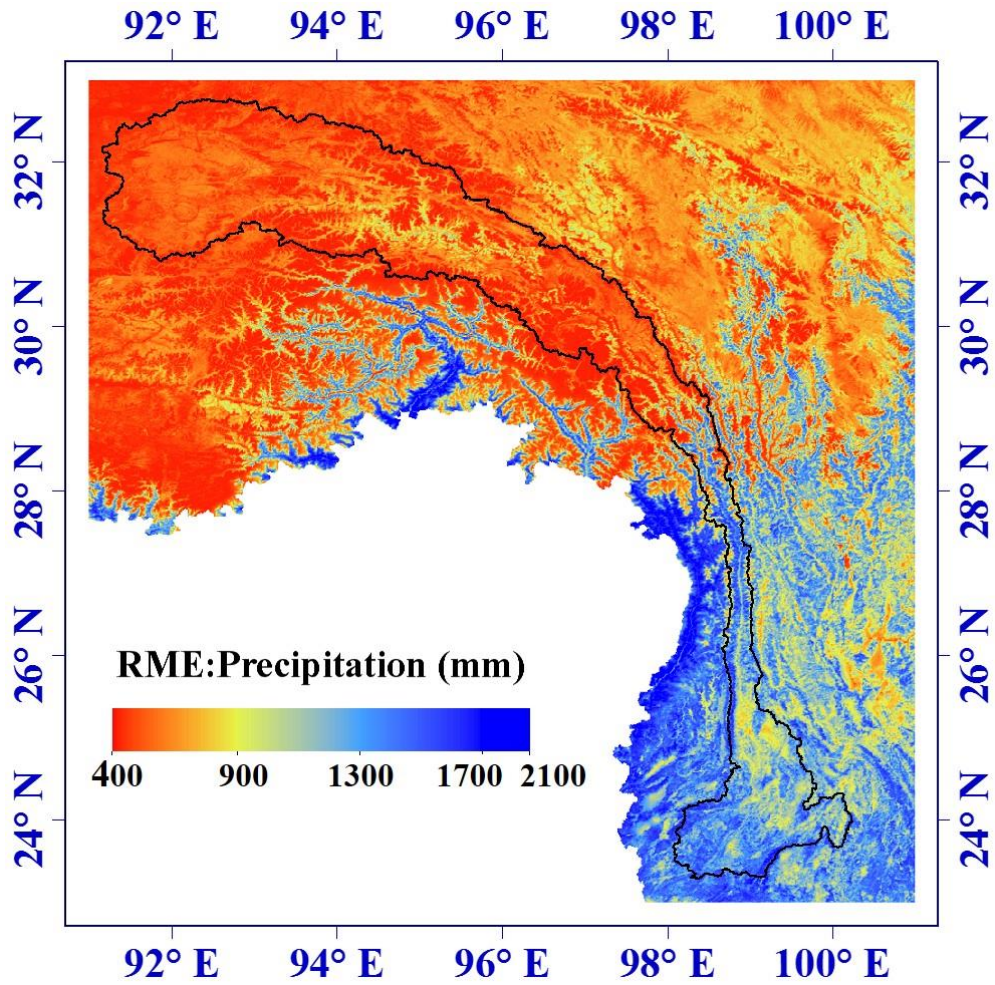
587

588 **Figure 7** The relationship between mean annual precipitation and NDVI at different elevation bands, (a) elevation

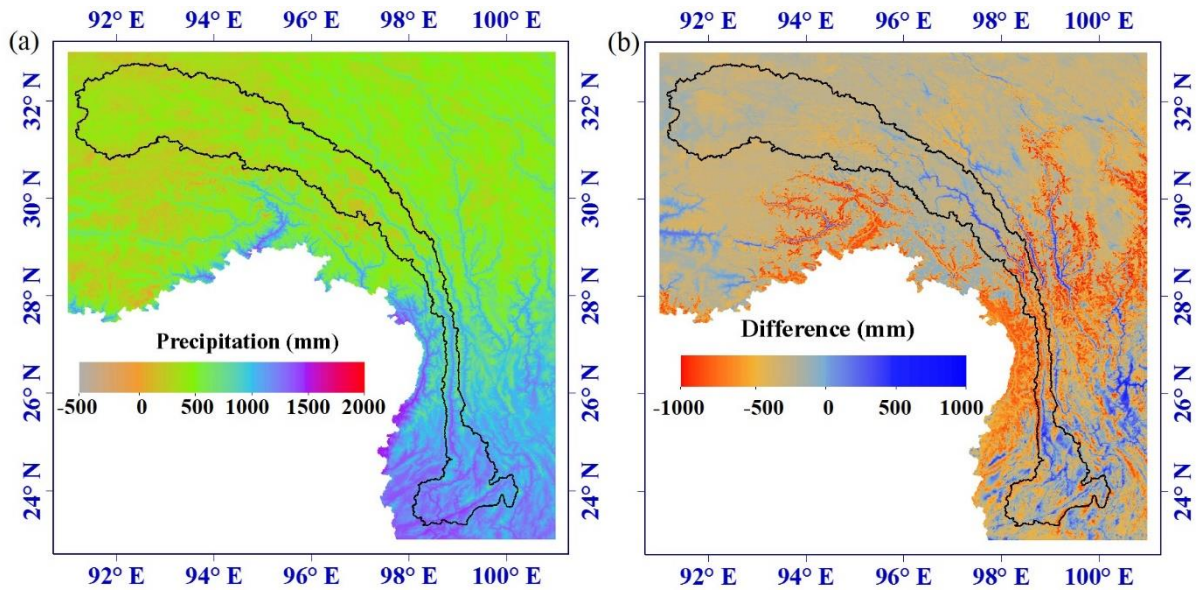
589 band : <200m; (b) band: 2000~3500 m; (c) band: >3500 m; (d) whole bands; (e) comparison of precipitation-

590 NDVI relationship for different bands .

591



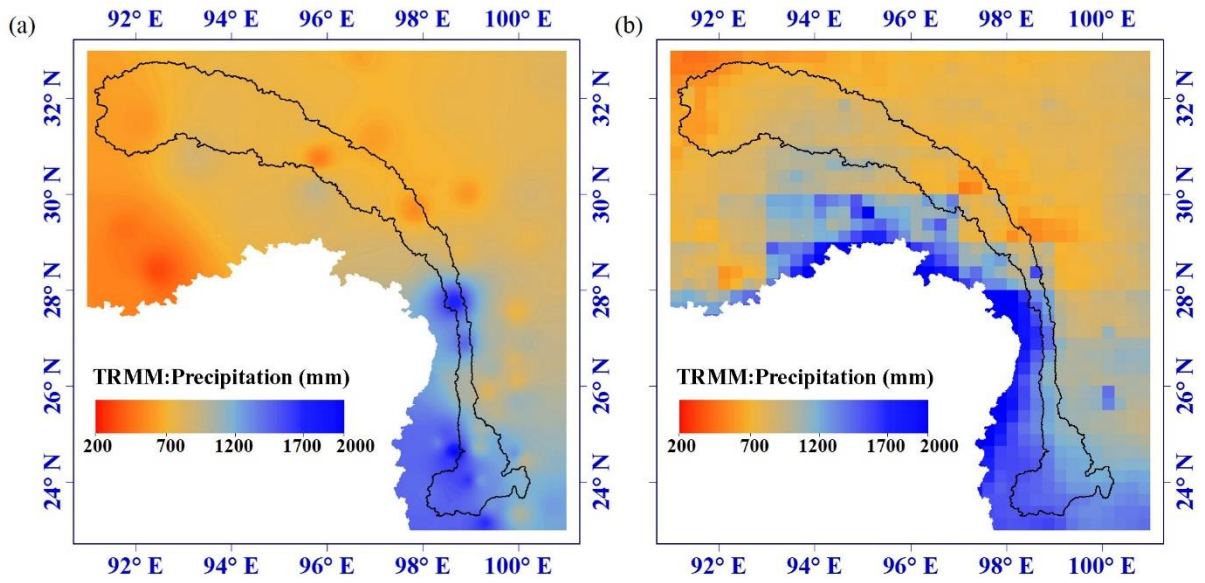
592
 593 **Figure 8** Average annual precipitation distribution of 2003-2012 from RME.
 594
 595



596
 597 **Figure 9** (a) The map of precipitation estimates of DEMP; (b) difference in precipitation estimates between
 598 RME and DEMP.

599

600



601

602

Figure 10 spatial distribution of mean annual precipitation of 2003-2012 estimated by (a) IDW and (b) TRMM.

603

604

605

606

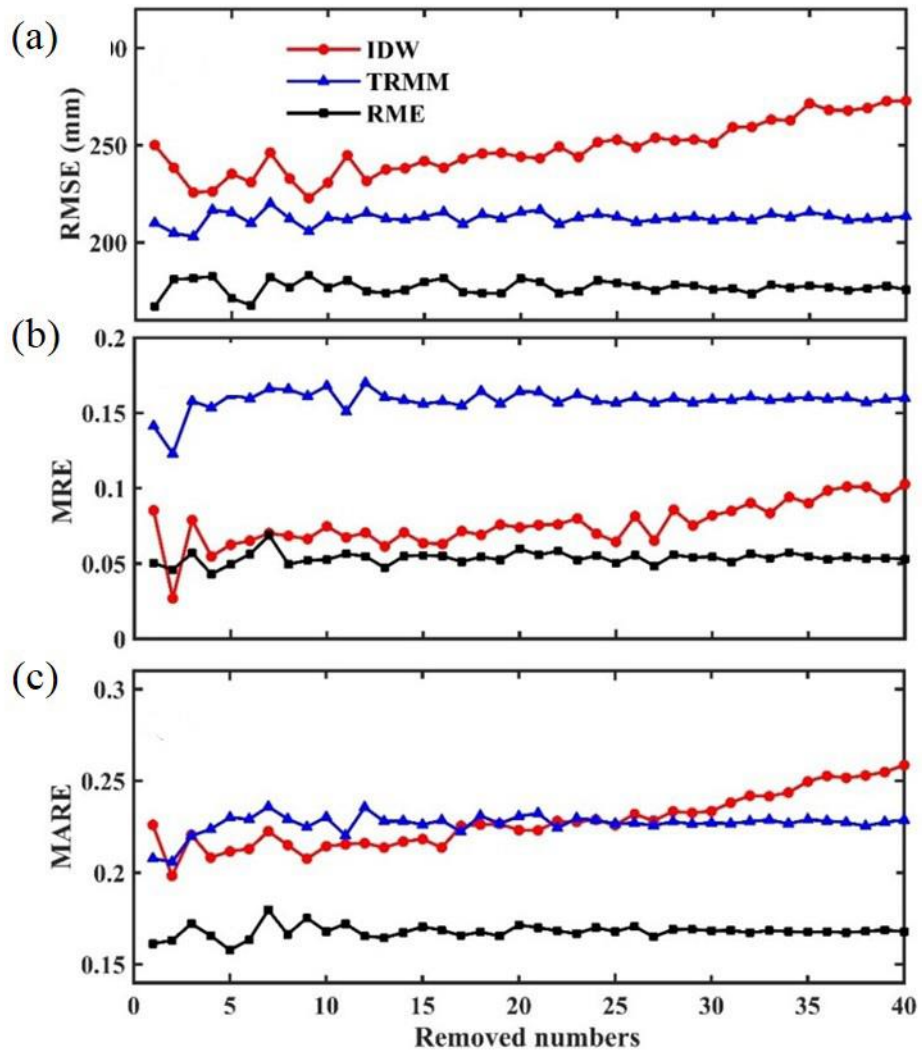
607

608

609

610

611



612

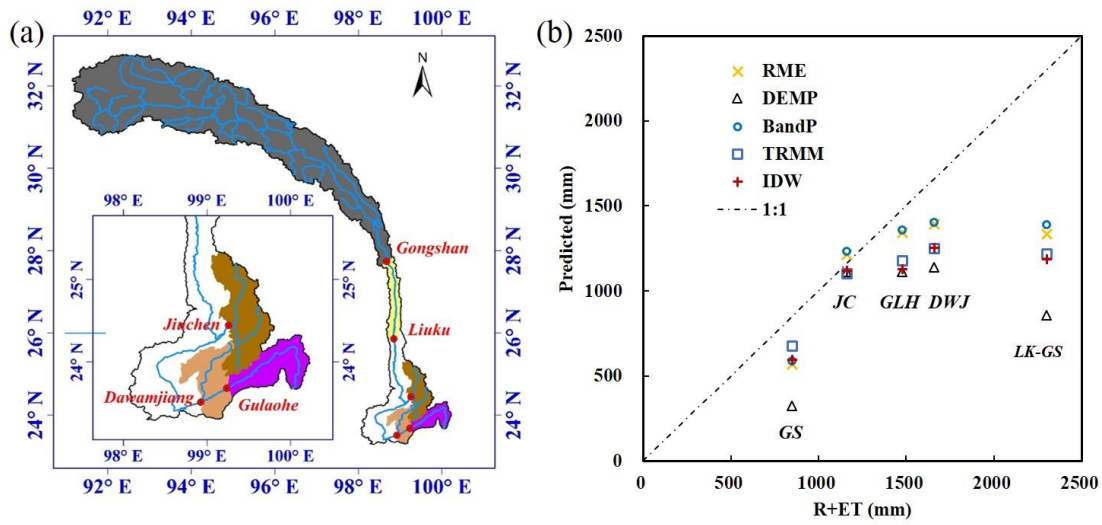
613 **Figure 11** Performance of E_{RMS} , E_{MR} and E_{MAR} for three methods in different remove numbers.

614

615

616

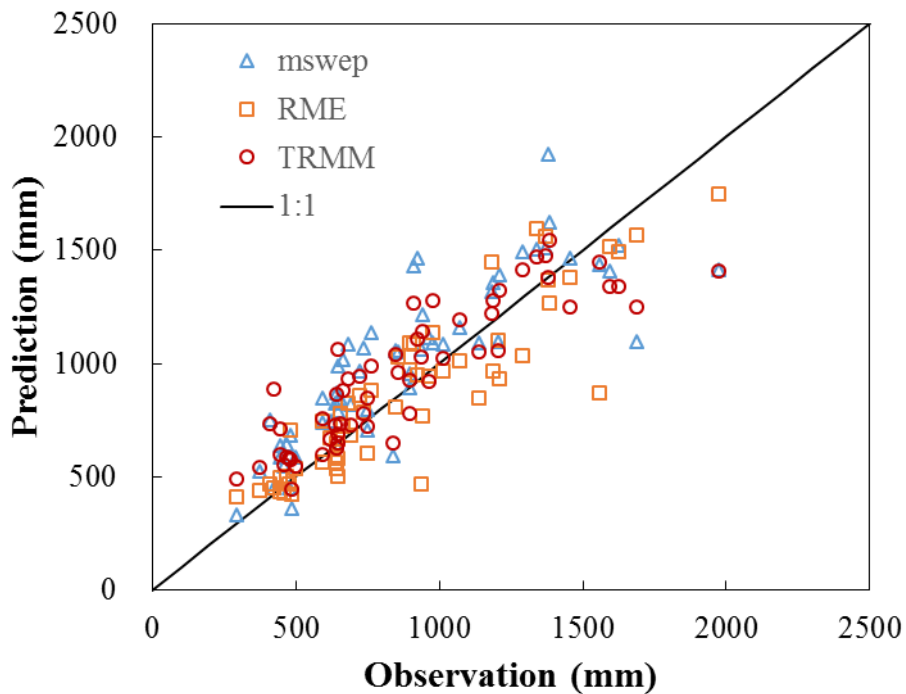
617



618

619 **Figure 12** (a) Sub-basins based on hydrological stations (b) Comparison between precipitations based on basin
 620 water balance (R+ET) and different annual rainfall products: DEMP (P-elevation relationship), BandP (P-NDVI
 621 relationship with consideration elevation band), RME, TRMM and IDW. GS, JC, GLH, DWJ and LK-GS are the
 622 abbreviations for Gongshan, Jiuchen, Gulaohu, Dawanjiang and Liuku-Gongshan, respectively.

623

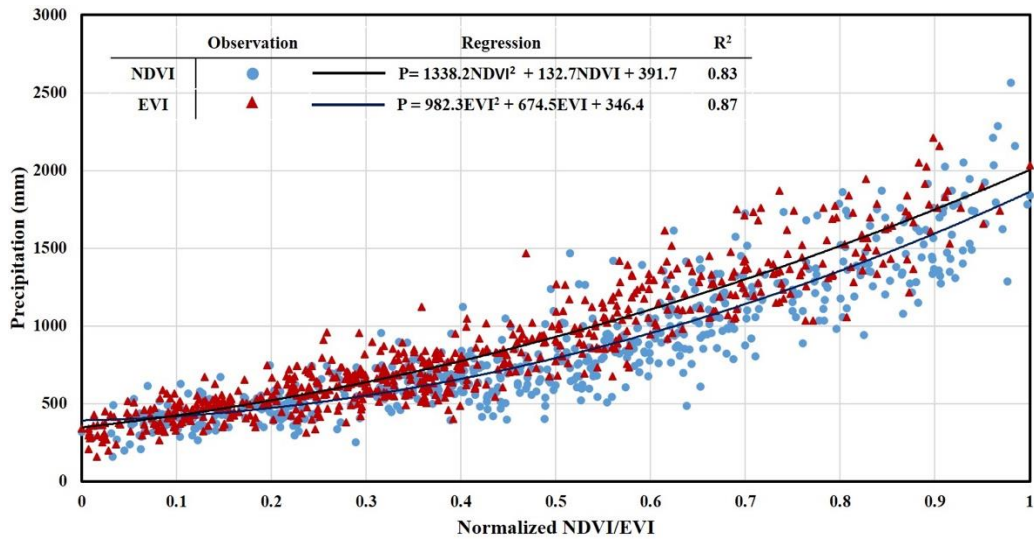


624

625 **Figure 13** Comparison in mean annual precipitation between the gauged measurements and predictions by the
 626 MSWEP, RMM and RME.

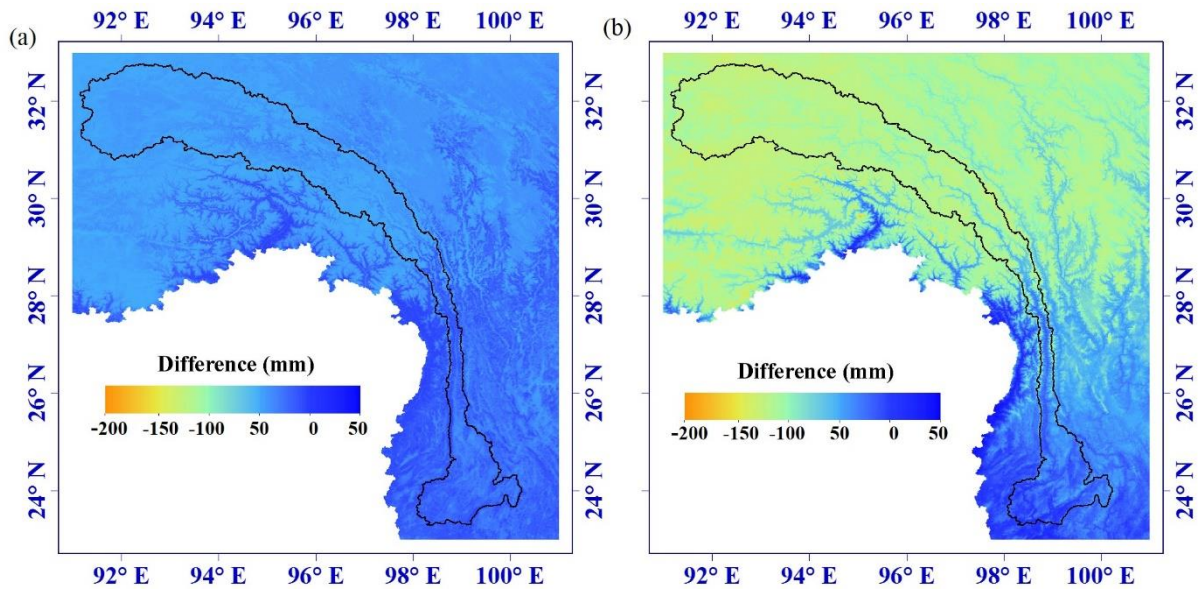
627

628



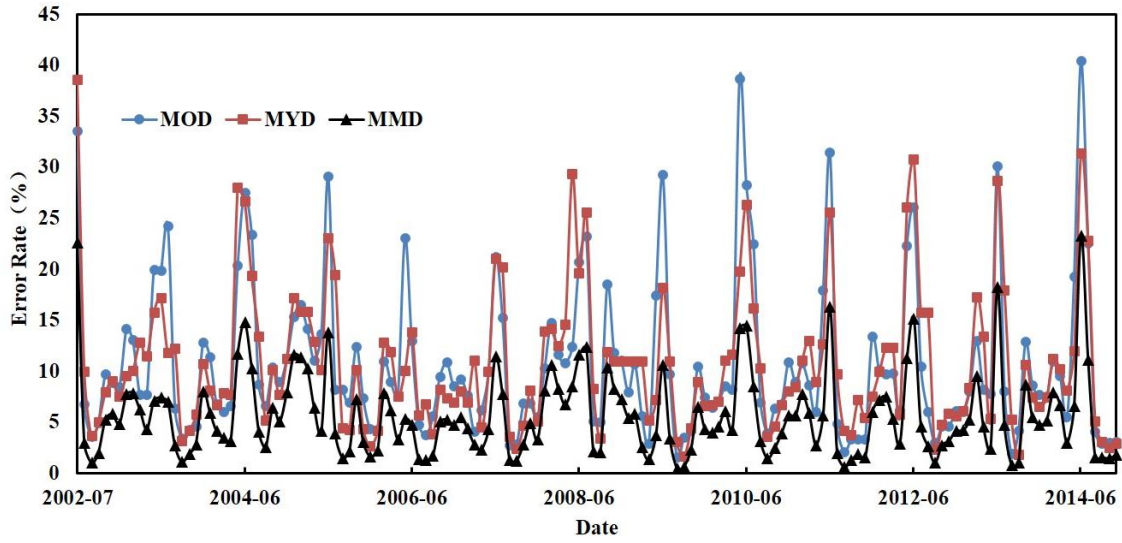
629
630
631
632
633

Figure 14 Regression relationship between annual precipitation and normalized NDVI/EVI



634
635
636

Figure 15 Spatial precipitation difference between RME and (a) RME+H; (b) RME+T(b).



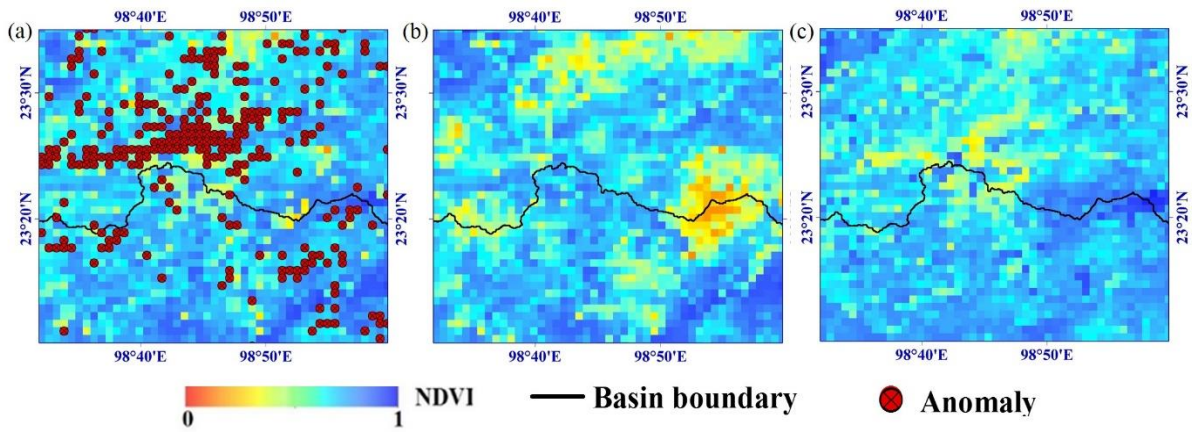
637

638 **Figure A1** Monthly Error rate of MOD, MYD and MMD

639

640

641

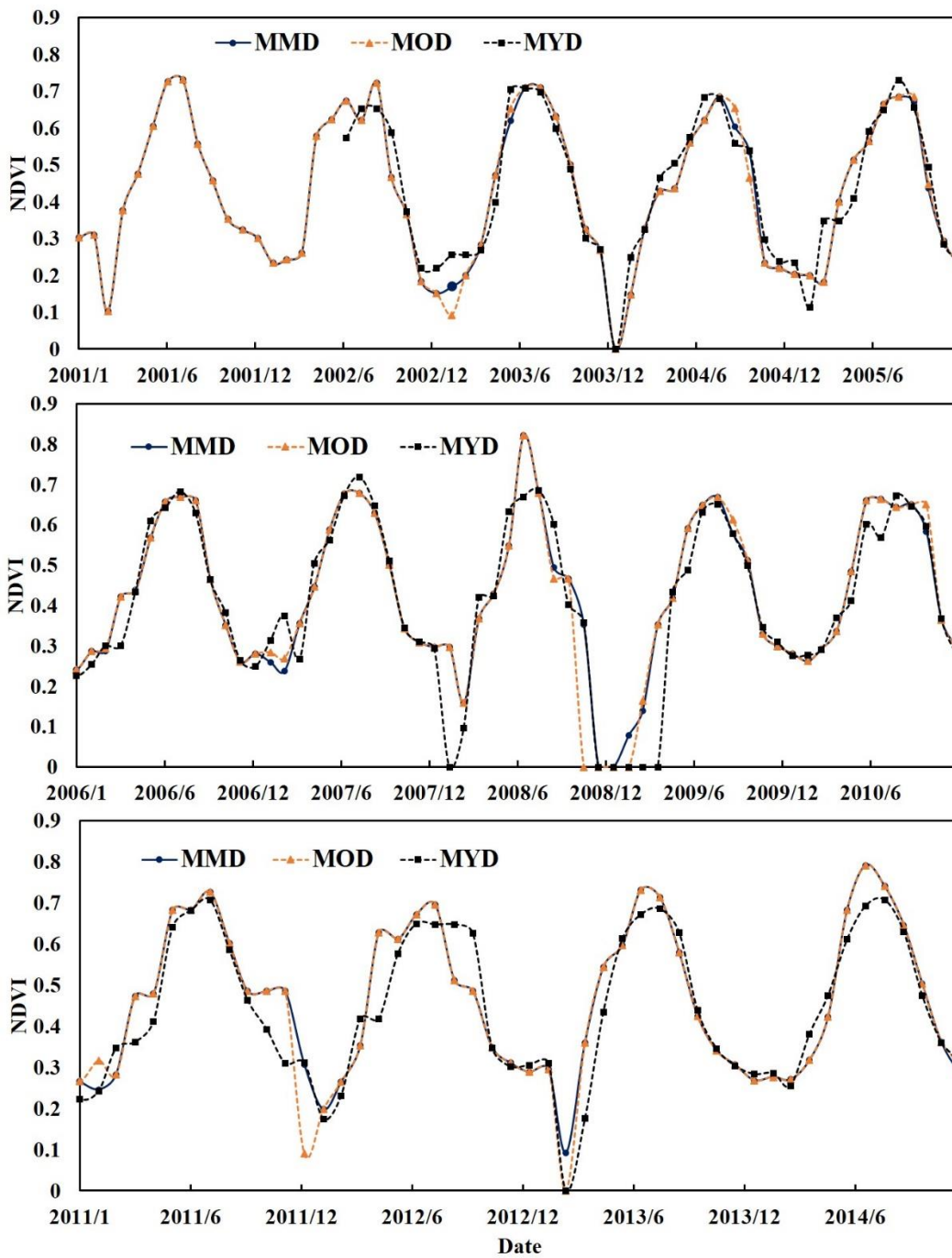


642

643 **Figure A2** Comparison of three NDVI products over a ridge area on June 2006, (a) for MMD, (b) for MOD, (c)

644 for MYD

645



646

647 **Figure A3** Comparison of three NDVI monthly times series over one gauge

648